Energy Agency, Vienna, 1968), Vol. 1, p. 149.
[6]J. R. D. Copley, B. N. Brockhouse, and S. H. Chen, in Ref. 5, p. 209.
[7]N. W. Ashcroft, Phys. Letters 23, 48 (1966).
[8]W. Shyu and G. D. Gaspari, Phys. Rev. 163, 667 (1967); 170, 687 (1968); 177, 1041 (1969).
[9]W. Shyu and G. D. Gaspari, Phys. Letters 30A, 53 (1969).
[10]J. Hubbard, Proc. Roy. Soc. (London) A240, 539 (1957); A243, 336 (1958).
[11]L. J. Sham, Proc. Roy. Soc. (London) A283, 33 (1965).
[12]W. Cochran, Proc. Roy. Soc. (London) A276, 308 (1963).
[13]The discussion is here formulated in terms of the test-charge–test-charge dielectric function, rather than in terms of the electron–test-charge dielectric function used in Refs. 8 and 9. For a discussion of this point, see, e.g., L. E. Ballentine, Phys. Rev. 158, 670 (1967).
[14]A. O. E. Animalu, Phil. Mag. 11, 379 (1965).
[15]D. J. W. Geldart and S. H. Vosko, Can. J. Phys. 44, 2137 (1966).
[16]R. W. Shaw, Jr., Ph. D. thesis, Stanford University, 1968 (unpublished).
[17]D. Weaire, Proc. Phys. Soc. (London) 92, 956 (1967).
[18]R. W. Shaw and N. V. Smith. Phys. Rev. 178, 985 (1969).
[19]H. C. Nash and C. S. Smith, J. Phys. Chem. Solids 9, 113 (1959).
[20]W. R. Marquardt and J. Trivisonno, J. Phys. Chem. Solids 26, 273 (1965).
[21]M. E. Diederich and J. Trivisonno, J. Phys. Chem. Solids 27, 637 (1966).
[22]C. A. Roberts and R. Meister, J. Phys. Chem. Solids 27, 1401 (1966).
[23]F. J. Kollarits and J. Trivisonno, J. Phys. Chem. Solids 29, 2133 (1968).
[24]S. H. Vosko, Phys. Letters 13, 97 (1964).
[25]F. G. Fumi and M. P. Tosi, J. Phys. Chem. Solids 25, 31 (1964).
[26]T. Schneider and E. Stoll, Physik Kondensierten Materie 5, 331 (1966).
[27]T. Schneider and E. Stoll, Solid State Commun. 5, 837 (1967).
[28]W. Cochran, in *Inelastic Scattering of Neutrons* (International Atomic Energy Agency, Vienna, 1965), Vol. 1, p. 3.

PHYSICAL REVIEW B VOLUME 3, NUMBER 2 15 JANUARY 1971

Compton Scattering and Electron Momentum Density in Beryllium*

R. Currat,† P. D. DeCicco, and Roy Kaplow
Center for Materials Science and Engineering, Massachusetts Institute of Technology, Cambridge, Massachusetts 02139
(Received 6 July 1970)

Compton-scattered x-ray spectra were measured for three orientations of a beryllium single crystal. The reduced profiles were analyzed in terms of the electron momentum distribution. Observed anisotropies can be explained qualitatively in terms of the geometry of the Fermi surface and are in qualitative agreement with earlier positron and x-ray data. The present results show high-momentum components among the valence electrons which are not revealed in the positron experiment nor accounted for by available calculations. In the process of reducing the data to obtain the momentum distribution of the valence electrons, detailed consideration was given to the effects of binding upon the Compton scattering by the core electrons.

I. INTRODUCTION

The energy distribution of inelastically scattered (Compton) x rays is of interest, in part because of its close relationship to the momentum-space electron wave functions in the scatterer. A measurement of the scattered x-ray energy spectrum provides a direct insight into the electron momentum distribution and (with single crystals) its anisotropies.

Earlier Compton work[1] and a positron annihilation study[2] on beryllium had indicated the existence of a number of anomalies, that is, of characteristics in the momentum profiles which were not predicted by the then available theoretical representations. These were variously attributed to such circumstances as (a) grossly altered 1*s* electron wave functions (compared to the free-atom state), (b) unexpectedly large high-momentum components among the conduction electrons, (c) inaccuracy of the scattering models, (d) uncertainties in the positron wave functions, (e) many-body effects, (f) experimental inaccuracies, and (g) inaccuracy in the data-reduction procedures. We have undertaken a repetition of the Compton measurements, striving for an accuracy which would allow a narrowing of the uncertainties.

II. EXPERIMENTAL TECHNIQUE

Measurements were made for three crystallographic directions on a single cube-shaped beryllium crystal; the x-ray scattering vector, $\vec{k} = \vec{k}_f$

$-\vec{k}_i$, was held parallel (nominally) to the $\langle 0001 \rangle$, $\langle 11\bar{2}0 \rangle$, and $\langle 1\bar{1}00 \rangle$ directions, respectively. The experimental arrangement is sketched in Fig. 1.

Mo $K\alpha$ radiation was used ($\lambda \simeq 0.71$ Å), at a scattering angle of 120°. The total divergence in the incident beam, defined by a Soller slit, was $\pm 2.5°$. At 120° the nominal Compton shift (for free electrons at rest) is 0.0364 Å, corresponding to an energy change of 850 eV, or 31.3 hartrees. A diffraction spectrometer was used for the energy analysis, with a LiF crystal of low mosaicity and fine Soller slits of comparable resolution. The (600) LiF reflection order was used for the $\langle 0001 \rangle$ and $\langle 11\bar{2}0 \rangle$ profiles; the (800) order, and correspondingly coarser slits, were used for the $\langle 1\bar{1}00 \rangle$ profile. The resolution of the spectrometer, measured in terms of the full width at half-height of the Mo $K\alpha_1$ peak, was ~0.00018 Å (~1.3 hartrees) or ~4% of the nominal Compton shift.

Bragg reflections of wavelengths from the continuous bremsstrahlung background (emitted by the x-ray tube) were avoided by offsetting the crystal (~3°) from the ideal reflecting orientations. Weak fluorescent lines due to impurities in the specimen crystal and to shielding were detected, identified (Pb, Ni, Cu), and subtracted from the recorded profiles.

The profiles were recorded in a 1024-channel multiscaler in which the channel advance had been synchronized to the forward motion of the spectrometer. The spectrometer was controlled by a device which provided an automatic slow-forward rapid-return sequence, the appropriate sweep-initiate trigger pulses for the multiscaler, and the electronic gating of the detected radiation pulses. Thus, a set of data was the accumulation of a large number of individual passes (each of about 20-min duration) and quite insensitive to source variations. In addition, a number of sets of data were obtained and summed for each crystal orientation. Alignment checks were interposed and gear rotations were used to guard against minor local distortions in the profile due to gear-tooth inaccuracy.

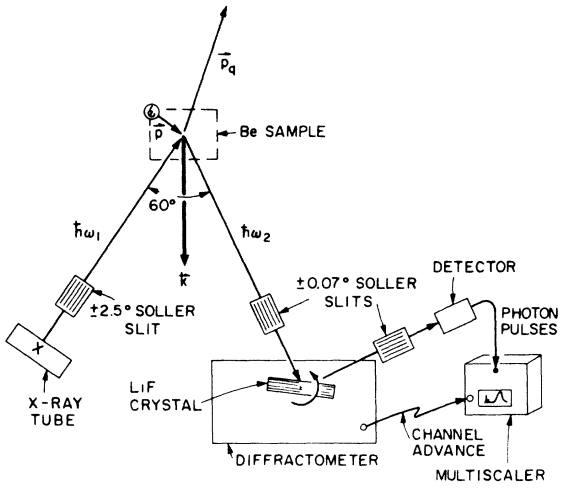

FIG. 1. Schematic diagram of experimental configuration.

The detector was a scintillation crystal (NaI-Tl) photomultiplier pair used with standard amplification and pulse-height discrimination electronics. The single-channel analyzer was set to obtain a minimal background, consistent with the necessity for a uniform sensitivity throughout the entire energy range of the experimental profile.

III. DATA REDUCTION

Ideally, we would consider the energy distribution after scattering, of initially monochromatic radiation. The primary data would then contain only the Compton profile of that radiation and the sharp unshifted peak of quasi-elastically scattered x rays (attributable, with crystalline specimens, to "thermal diffuse scattering"). However, besides the Mo $K\alpha_1$, the incident beam contains the aforementioned bremsstrahlung and also other molybdenum radiation. Such radiations contribute to the measured pattern to the extent that they scatter from the specimen, are diffracted by the analyzing crystal (in any order), and passed by the pulse-height analyzer. Bragg reflections from the bremsstrahlung are readily avoided (with single-crystal specimens), and impurity peaks subtracted; however, extraneous contributions do arise from the Mo $K\alpha_2$ and from diffusely (elastic and inelastic) scattered bremsstrahlung. Subtraction of the slowly varying background contributed by the latter is complicated by the fact that a number of reflection orders are involved. The analyzing crystal reflectivity varies across the angular range used; the variation is slight but not insignificant and depends on the order of reflection. In order to minimize uncertainties, the reflection order (or wavelength) composition of the intensity was measured at several points under and in the vicinity of the Compton line, using calibrated Au, Va, and Al absorbers in the path of the beam. With the LiF crystal being used in the (600) order and the pulse-height analyzer set to accept uniformly all wavelengths from 0.7 to 0.8 Å, the following characteristics were measured:

(i) The non-(600) contribution appears to be linear under the Compton line and is responsible for about $\frac{2}{3}$ of the background and virtually all of its slope.

(ii) The (200) bremsstrahlung background is eliminated by the pulse-height discrimination.

(iii) The (1000) and higher-order reflections are too inefficiently diffracted to contribute appreciably.

(iv) The (400) component decreases with wave-

length and the (800) increases slightly, both consistent with the hypothesis that the variation is primarily due to the pulse-height discrimination.

After subtraction of the non-(600) background, the following reductions were applied:

(i) correction for the wavelength dependence of absorption in the sample and of the LiF crystal reflectivity (both quite small – a few percent);

(ii) subtraction of (600) background, i.e., of the nearly constant intensity below the *peaks* of modified and unmodified radiation;

(iii) separation of the Mo$K\alpha_2$ component. The Rachinger[3] method was used with an experimentally determined α_2/α_1 ratio of 0.525 ($\pm$0.015).

The data reduction involved no free parameters except for one normalization constant, and no presumptions regarding the shape or symmetry of the Comption profile.

IV. THEORY

The Compton scattering of x rays with energy $\hbar\omega_1 \leq 0.04mc^2$ by electrons in a solid gives rise to electron recoil energies which are typically $\leq 4(\hbar\omega_1/c)^2/2m$ or $0.003mc^2$. Thus for solids composed of light atoms, both the initial and final states of the electronic system may be described nonrelativistically. The coupling of the electronic system to the electromagnetic field is then described by $\vec{p}\cdot\vec{A}$ and A^2 interaction terms, where $\vec{p}$ is the electron momentum and $\vec{A}$ is the vector potential of the radiation. The $\vec{p}\cdot\vec{A}$ term appears to be negligible.[4-6] Consideration of the A^2 term alone to first order gives, for an N-electron system, the differential scattering cross section

$$\frac{d\sigma}{d\Omega\, d\omega} = \left(\frac{d\sigma}{d\Omega}\right)_{\mathrm{Th}} \frac{\omega_2}{\omega_1} \sum_q \left| \langle q | \sum_{j=1}^{N} e^{i\vec{k}\cdot\vec{r}_j} | 0 \rangle \right|^2 \times \delta(\epsilon_q - \epsilon_0 - \omega), \tag{1}$$

where $(d\sigma/d\Omega)_{\mathrm{Th}} = (e^2/mc^2)^2(\vec{e}_1\cdot\vec{e}_2)^2$ is the Thompson scattering cross section of the electron, and $\omega = \omega_1 - \omega_2$ and $\vec{k} = \vec{k}_1 - \vec{k}_2$ are, respectively, the energy and momentum transferred by the photon to the system whose initial and final states are $|0\rangle$ and $|q\rangle$, respectively. $\delta(\epsilon_q - \epsilon_0 - \omega)$ states the energy-conservation condition. (We have used atomic units with $\hbar = m = 1$.)

The cross section given by Eq. (1) is basically the one previously used[1,4,5] in the discussion of the Compton profile, except that the factor ω_2/ω_1 is often dropped; it is approximately equal to 0.95 at the center of the Compton peak in our case.

A. Impulse Approximation

An approximation to Eq. (1) has been derived,[5] which is referred to as the "impulse approximation":

$$\frac{d\sigma}{d\Omega\, d\omega} = \left(\frac{d\sigma}{d\Omega}\right)_{\mathrm{Th}} \frac{\omega_2}{\omega_1} \frac{V}{(2\pi)^3} \int \delta(\tfrac{1}{2}k^2 + \vec{p}\cdot\vec{k} - \omega) \times \langle 0 | n_{\vec{p}} | 0 \rangle\, d\vec{p}, \tag{2}$$

where $\langle 0|n_{\vec{p}}|0\rangle$ is the probability of finding an electron with momentum $\vec{p}$ and $[V/(2\pi)^3]\int d\vec{p}$ represents the sum over momentum eigenstates. This approximation is exact for free electrons and valid in the limit of a slowly varying potential. We will therefore apply Eq. (2) to the scattering from valence (conduction) electrons, but will give further consideration to scattering from core electrons.

Since the experimental data do not give us $d\sigma/d\Omega\, d\omega$ on an absolute scale, it is necessary to normalize the experimental curve so that $d\sigma/d\Omega$ assumes its theoretical value. To obtain the valence contribution to $d\sigma/d\Omega$ we integrate Eq. (2) with respect to ω and obtain

$$\left(\frac{d\sigma}{d\Omega}\right)_{\mathrm{val}} = \left(\frac{d\sigma}{d\Omega}\right)_{\mathrm{Th}} \frac{V}{(2\pi)^3} \int d\vec{p}\, \langle 0|n_{\vec{p}}|0\rangle \times \left(\frac{\omega_2}{\omega_1} \frac{1}{1 - (\vec{k}+\vec{p})\cdot(d\vec{k}/d\omega)} \right)\Bigg|_{\omega = k^2/2 + \vec{p}\cdot\vec{k}} \tag{3}$$

From the definitions of $\vec{k}$ and ω we have

$$k^2 = 4k_1^2 \sin^2\theta \left(1 - \frac{\omega}{\omega_1} + \frac{\omega^2}{4\omega_1^2 \sin^2\theta}\right). \tag{4}$$

If we now retain terms of order ω/ω_1 in comparison to unity but neglect terms of higher order in ω/ω_1, and make use of the inversion symmetry of $\langle 0|n_{\vec{p}}|0\rangle$ to eliminate linear terms in $\vec{p}$, we obtain

$$\left(\frac{d\sigma}{d\Omega}\right)_{\mathrm{val}} = \left(\frac{d\sigma}{d\Omega}\right)_{\mathrm{Th}} n_{\mathrm{val}} \left(1 - \frac{k_0^2}{2\omega_1}\right)^2, \tag{5}$$

where n_{val} is the number of valence electrons and $\frac{1}{2}k_0^2$ is the energy transfer for Compton scattering of an x ray of frequency ω_1 through an angle 2θ (120° in this instance) by a free electron initially at rest. Apart from terms of order $(\omega/\omega_1)^2$, the result of Eq. (5) agrees with the Klein-Nishina formula[7] for the Compton cross section of a free electron at rest. Although the total cross section of Eq. (5) follows from the impulse approximation for an arbitrary ground-state distribution $\langle 0|n_{\vec{p}}|0\rangle$, it will contain an unphysical contribution corresponding to negative energy transfer from the region $\frac{1}{2}k^2 + \vec{p}\cdot\vec{k} < 0$, if $\langle 0|n_{\vec{p}}|0\rangle$ is nonzero in this region. In our case $k \cong 8$ a.u., while the free-electron Fermi momentum for Be is 1.027 a.u., so that we would expect this unphysical contribution to the total Compton scattering by the valence electrons to be negligible.

B. Core Contribution

To calculate the contribution of a core electron

to $d\sigma/d\Omega$ we observe from Eq. (1) that we need the matrix element of $e^{i\vec{k}\cdot\vec{r}}$ between the final state $|q\rangle$ and the initial state $|0\rangle$. Since the initial-state wave function is concentrated close to the nucleus, the result may be sensitive to the behavior of the final-state wave function in that region. We should therefore obtain $d\sigma/d\Omega$ from a calculation of $d\sigma/d\Omega\,d\omega$ in which appropriate final-state wave functions are used. Alternatively, we may temporarily bypass the final-state problem; we can formally integrate Eq. (1) with respect to ω and obtain

$$\frac{d\sigma}{d\Omega}=\left(\frac{d\sigma}{d\Omega}\right)_{\mathrm{Th}}\sum_q\left(1-\frac{\omega}{\omega_1}\right)\langle 0|e^{-i\vec{k}\cdot\vec{r}}|q\rangle \times\langle q|e^{i\vec{k}\cdot\vec{r}}|0\rangle\Big|_{\omega=\epsilon_q-\epsilon_0}, \tag{6}$$

where, since the direction of $\vec{k}_2$ is fixed, the ω dependence of $\vec{k}$ is given by

$$\vec{k}=\vec{k}_1-(\vec{k}_2/\omega_2)(\omega_1-\omega). \tag{7}$$

If we now neglect first-order terms in ω/ω_1 and assume that the initial state $|0\rangle$ plus the possible final state $|q\rangle$ form a complete set, we obtain the Waller-Hartree result for the total cross section[4]

$$\frac{d\sigma}{d\Omega}=\left(\frac{d\sigma}{d\Omega}\right)_{\mathrm{Th}}(1-|\langle 0|e^{-i\vec{k}\cdot\vec{r}}|0\rangle|^2)=\left(\frac{d\sigma}{d\Omega}\right)_{\mathrm{Th}}(1-f^2), \tag{8}$$

where f is the x-ray form factor for the core state. In the limit of weak binding ($f\to 0$), the core contribution to $d\sigma/d\Omega$ should approach the free-electron result of Eq. (5). Thus an approximate way to recover the first-order terms in ω/ω_1 is

$$\left(\frac{d\sigma}{d\Omega}\right)_{\mathrm{core}}=\left(\frac{d\sigma}{d\Omega}\right)_{\mathrm{Th}}(1-f^2)\left(1-\frac{\omega^*}{\omega_1}\right)^2, \tag{9}$$

where ω^* is a suitable average value for the energy transfer, such as the value at the center of the Compton profile.

To begin a theoretical interpretation of normalized data, we will assume that the core contribution to the Compton scattering is essentially the same in the solid state as it is in the isolated atom. This assumption is supported by the results of some modifications of the atomic calculation of the core contribution described below.

In the usual Hartree-Fock or other self-consistent-field atomic calculations, each one-electron orbital $\psi_i(\vec{r})$ may be regarded as a solution of Schrödinger's equation for a particle in a spherical potential $V_i(r)$. $V_i(r)$ is approximately (or exactly in the case of the Hartree approximation) the Coulomb potential produced by the nucleus and the charge densities of other occupied orbitals. We assume initially that a Compton event which removes an electron from an orbital $\psi_i(\vec{r})$ will leave the electron in a recoil state whose wave function also satisfies Schrödinger's equation for the same potential $V_i(r)$. We can then write the recoil-state wave function as $\psi_q(\vec{r})=g_l(r;\epsilon)Y_l^m(\theta,\phi)$, where the function $g_l(r;\epsilon)$ is determined by numerical integration outward from $r=0$ of the radial Schrödinger equation

$$\left(-\frac{1}{2}\frac{d^2}{dr^2}+V(r)+\frac{l(l+1)}{2r^2}-\epsilon\right)rg_l(r;\epsilon)=0\ . \tag{10}$$

From Eq. (1) the differential cross section for Compton scattering from a core electron initially in the state $\psi_i(\vec{r})$ is given by

$$\frac{d\sigma}{d\Omega\,d\omega}=\left(\frac{d\sigma}{d\Omega}\right)_{\mathrm{Th}}\frac{\omega_2}{\omega_1}\sum_{lm}\frac{dn}{d\epsilon}\left|\int g_l(r;\epsilon) \times Y_l^{*m}(\theta\phi)e^{i\vec{k}\cdot\vec{r}}\psi_i(\vec{r})\,d^3r\right|^2, \tag{11}$$

where $\epsilon=\epsilon_i+\omega$ and $dn/d\epsilon$ is the number of states per unit energy with quantum numbers l and m. To determine $dn/d\epsilon$ and the normalization of $g_l(r;\epsilon)$, the final states were confined to a sphere of arbitrarily large radius and the WKB approximation was used to continue the numerical function $g_l(r;\epsilon)$ out to a suitably large value of r. Since $\psi_i(\vec{r})$ is generally taken to be an eigenfunction of angular momentum, the integral in Eq. (11) is easily reduced to one or more radial integrations by using the partial-wave expansion of $e^{i\vec{k}\cdot\vec{r}}$. In our case the core electron is initially in an s state, so that Eq. (11) becomes

$$\frac{d\sigma}{d\Omega\,d\omega}=\left(\frac{d\sigma}{d\Omega}\right)_{\mathrm{Th}}\frac{\omega_2}{\omega_1}\sum_{l=0}^{\infty}4\pi(2l+1)\frac{dn}{d\epsilon}\left|\int g_l(r;\epsilon) \times j_l(kr)\psi_s(r)\,r^2dr\right|^2. \tag{12}$$

As an over-all check on the numerical computation outlined above, we have applied Eq. (12) to the hydrogenic 1s state of Be^{+++}, obtaining agreement with an exact analytic calculation[8] to within a few parts in 10^4.

As a first calculation of the Compton scattering from the 1s electrons in the Be atom we used the atomic potential of Herman and Skillman[9] for both the initial and final states. This result is shown as curve (d) in Fig. 2. That calculation was followed by a series of calculations in which we investigated the sensitivity of the result to certain characteristics of the potential and attempted to simulate some of the effects to be expected from the crystalline environment, but always using the same potential for the final state as for the initial state. One modification consisted of eliminating the $-1/r$ tail of the Herman-Skillman potential outside the atomic radius. Another consisted of using the potential from a previous energy-band calculation[10] which included the spherically averaged effect of neighbor-

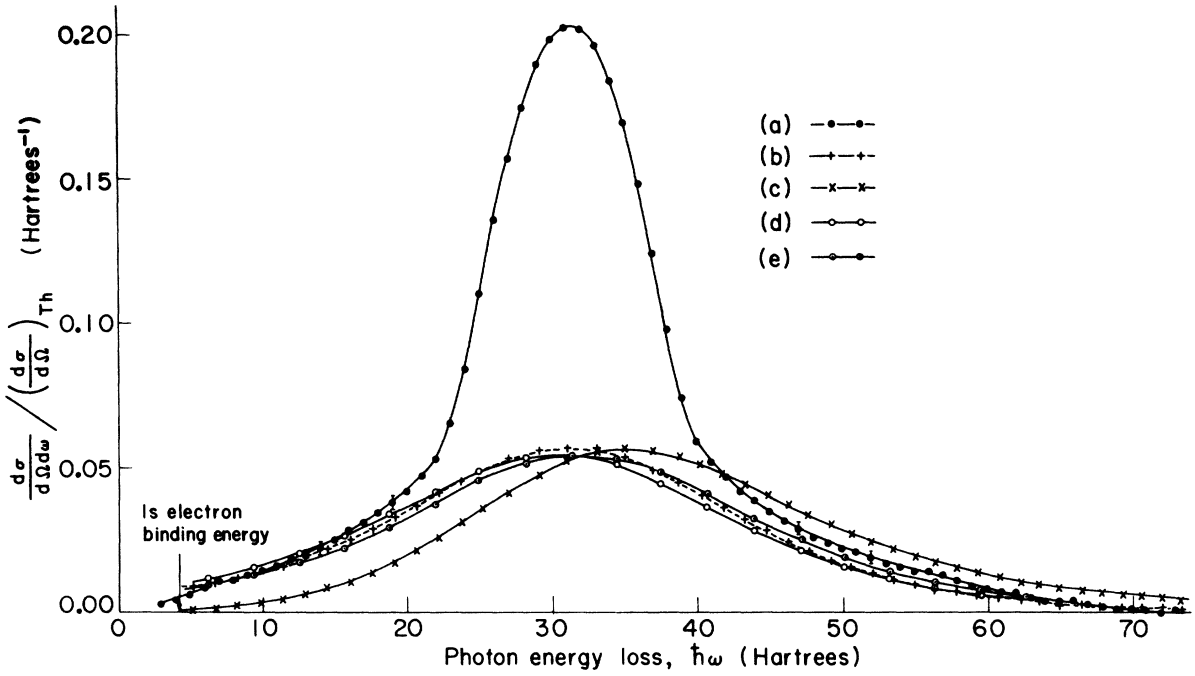

FIG. 2. Experimental Compton profile (average of three directions) and core calculations: (a) experimental curve; (b) Clementi Be 1s and impulse approximation; (c) Clementi Be 1s and plane-wave final state; (d) Herman-Skillman potential for initial and final states; (e) same as (d) with 1s Coulomb potential added to final-state potential.

ing atoms. The effect of shifting the potential with respect to the zero potential at infinity was investigated, as well as the effect of introducing a large dip in $V(r)$ at values of r in the vicinity of the nearest-neighbor distance in the crystal. None of these various potentials caused changes in the calculated Compton profile for the 1s electrons of as much as 1% for values of the energy transfer more than 5 hartrees above threshold. Larger differences were found only close to threshold (5% at 2 hartrees above), where the energies of the recoil states are small. This relative insensitivity of the Compton profile to those changes described above is a reflection of the fact that there was actually very little alteration of the potential, other than a constant shift, in the small region where the 1s wave function is large.

The area of the Compton profile for a Be 1s electron, using the Herman-Skillman potential, was found by an approximate numerical integration to be $0.86(d\sigma/d\Omega)_{\mathrm{Th}}$ as compared with $0.867(d\sigma/d\Omega)_{\mathrm{Th}}$ from Eq. (9).

In view of the small size of the first Bohr radius ($\cong 0.25$ a.u.), it does seem reasonable to assume that a localized 1s state in the crystal is the solution of Schrödinger's equation for a spherical potential much like the atomic potential. We also assume that the 1s profile does not depend on whether the form of the recoil wave function outside the atom is that of a continuum state of an isolated atom or a superposition of Bloch functions appropriate for a crystal. In view of the insensitivity of the calculated 1s profile to the changes in potential described above, this assumption appears reasonable It is also supported by the fact that the assumption of plane waves and of free-particle spherical waves for the recoil state leads to identically the same result.

However, the assumption that the same potential should be used for the recoil state as for the 1s state is clearly open to question. In calculating the potential seen by the recoiling electron one might use orbitals for the remaining electrons which are "relaxed" to the absence of a 1s electron. We can estimate this effect in the isolated atom by noting that the Coulomb potential at the nucleus produced by the two 2s electrons is $\langle 2s \mid 2/r \mid 2s \rangle$ or $2Z_{eff}/n^2$, where Z_{eff} is the effective nuclear charge seen by the 2s electrons and n, the principal quantum number, is 2. The change in Z_{eff} due to removing one 1s electron is $\cong 1$, so that the change in the Coulomb potential at $r = 0$ due to relaxation of the 2s orbitals is $\simeq 0.5$ hartrees. For the remaining 1s electron, the change in Z_{eff} would be about 0.3, [11] so that the Coulomb potential at $r = 0$ due to this electron would change by about 0.3 hartrees. Thus in the core

region, the potential for the initial 1*s* state is on the average 0.6 or 0.7 hartrees deeper than the potential for the recoil state. Taking this change in potential to be a constant over the core region, which is a reasonable approximation for the part coming from the 2*s* shell, we can deduce the change of the Compton profile from our previous calculations. We have seen that a shift of the potential for both the 1*s* and recoil states in the core region results in essentially no change in the Compton profile. Thus the upward shift of the final potential is equivalent to a downward shift of the initial potential and of the 1*s* energy. Thus from Eq. (11), which gives the Compton profile as a function of $\epsilon = \epsilon_i + \omega$, we see that the Compton profile is shifted toward larger ω by 0.6–0.7 hartrees. The lowering of the total energy of the remaining electrons due to relaxation would cut that shift approximately in half, but in the crystal, the Be core is surrounded by a higher concentration of valence electrons so that a larger relaxation effect may be expected. An extreme relaxation limit can be reached by making the rather implausible assumption that the hole in the 1*s* shell is filled by surrounding electrons so that the potential for the recoil state is the Coulomb potential of a neutral Be atom. The result of a similar calculation in which the recoil-state potential differs from the initial-state Herman-Skillman potential by the addition of the Coulomb potential produced by a 1*s* electron is shown as curve (e) in Fig. 2. An alternative interpretation of such a calculation would be that the Compton process produces a Bloch 1*s* hole, rather than a localized one, and that the exchange potential for the recoil Bloch state would be much weaker than the exchange potential for the 1*s* state. The addition of the Coulomb potential of a 1*s* electron to the potential in the core region has approximately the effect of removing the exchange hole from the potential in that region.

V. EXPERIMENTAL RESULTS AND DISCUSSION

The experimental profiles, processed as described in Sec. III, were normalized according to Eqs. (5) and (9):

$$\left(\frac{d\sigma}{d\Omega}\right)_{\text{tot}} = \left(\frac{d\sigma}{d\Omega}\right)_{\text{val}} + \left(\frac{d\sigma}{d\Omega}\right)_{\text{core}} = 3.54\left(\frac{d\sigma}{d\Omega}\right)_{\text{Th}} . \quad (13)$$

A cursory comparison of the results for the three directions shows that, while significant differences exist in the central regions, the tails are nearly identical. The latter regions (beyond ~ 2 a.u.) correspond to high initial electron momenta and are primarily core contribution. For that portion the deviations among the three directions are less than 1% of the maximum intensity and we attribute them to experimental and data-reduction uncertainties, rather than to core (or high-momentum valence) anisotropy. Symmetry considerations in the central region indicate the possibility of errors of similar magnitude within a single profile, also. It should be noted, however, that neither of these comparisons in themselves preclude the possibility of a small but consistent distortion of the symmetry of the tail portion of all three profiles.

The differences among the three direction profiles in the central region are directly related to the anisotropy in the valence momentum distribution. We can examine that effect without consideration of the core if we assume the latter electrons to be isotropic. In the impulse approximation, Eq. (2), the integral for a given ω is taken over the plane in momentum space defined by the conservation relationship

$$\vec{p}\cdot\vec{k} = \omega - \tfrac{1}{2}k^2 . \quad (14)$$

It is convenient to refer to the momentum component along the scattering vector as the independent variable z defined by

$$z = \vec{p}\cdot\vec{k}/k = \omega/k - \tfrac{1}{2}k \quad (15)$$

and to note that the variation of

$$\omega_2/\omega_1 k \approx (2k_1 \sin\theta)^{-1}(1 - \omega/2\omega_1) \quad (16)$$

across the valence peak is slight. In that approximation, therefore, the valence $d\sigma/d\Omega d\omega$ is predicted to be roughly an even function of z, $J(z)$.

The difference

$$\delta(z) = J^{(z)}_{0001} - J^{(z)}_{11\bar{2}0} ,$$

which shows the greatest anisotropy, is plotted in Fig. 3. The difference shown is the average of the

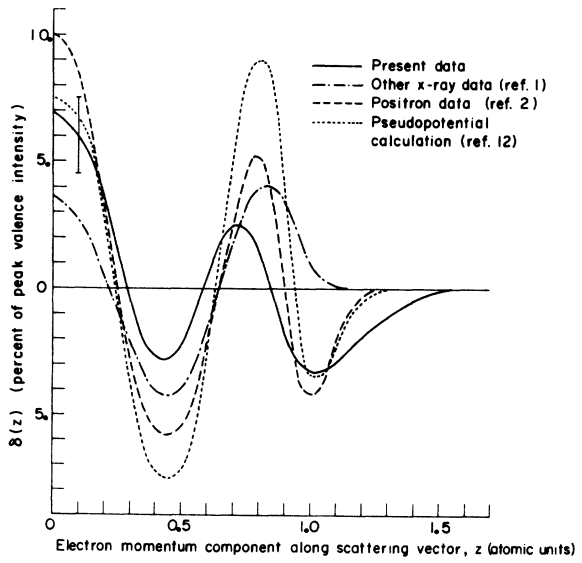

FIG. 3. Anisotropy between ⟨0001⟩ and ⟨11$\bar{2}$0⟩ directions.

$\pm z$ sides and the error bar indicates the maximum discrepancy in the symmetry about $z = 0$.

In Fig. 3 we also show the same difference function derived from previous x-ray measurements, [1] from positron annihilation measurements, [2] and from a pseudopotential calculation. [12] Qualitative agreement exists among all the results. The two x-ray measurements, although not in good mutual agreement, both indicate a smaller anisotropy than the positron result and the pseudopotential calculation. With respect to the positron data the difference might be due to the fact that x rays and positrons do not have the same spatial probability densities. It is generally assumed that the x-ray intensity is uniform within the material, an assumption which is probably equivalent to ignoring any dynamic scattering effects. It is expected, and verified by the relatively small core contributions in the positron results, that the positron probability density is nonuniform and significantly larger in the space between the cores. That bias would tend to give an overestimation of the anisotropy in positron data. On the other hand, the pseudopotential calculation predicts as large or larger anisotropies. It would be interesting to see if anisotropies of that magnitude persist with the inclusion of additional potential coefficients in that calculation, or in other calculations which take more direct account of the crystal potential. A qualitative interpretation of the anisotropy may be made on a simple geometric basis as well, which also serves to relate these data to the specific structure of crystalline beryllium. For that purpose we use a quasi-free-electron approach in which we assume that the distribution of momenta is the same as the distribution of occupied $\vec{k}$ states, using as the limiting surface not the free-electron Fermi sphere but the actual Fermi surface. [13] In that approximation the integral of Eq. (14) is proportional to the cross-sectional area of the occupied volume in k space. In the present case this volume consists primarily of the first and second zones, plus small electron pockets in the third zone (the "cigars") and minus compensating holes in the second zone (the "coronet"). A section of the occupied volume containing the points Γ and Σ [Fig. 4(c)] has a smaller area than a section through the basal plane [Fig. 4(b)]. Hence $\delta(z)$ is positive near $z = 0$. As z increases, $J_{11\bar{2}0}$ remains almost constant until $z = \frac{1}{2}\Gamma K = 0.48$ a.u. This is due to the nearly cylindrical shape of the polyhedron in the $(11\bar{2}0)$ direction. Beyond that point $J_{11\bar{2}0}$ decreases quite rapidly. J_{0001}, on the contrary, decreases at a constant rate from $z = 0$ to $z = 0.9$. This accounts for the minimum in $\delta(z)$ at $z \cong 0.45$ and the maximum at $z \cong 0.75$. In the vicinity of the Fermi momentum J_{0001} vanishes rapidly as the intersecting plane crosses the top face of the zone, whereas $J_{11\bar{2}0}$ benefits from the contribution of the "cigars." Hence

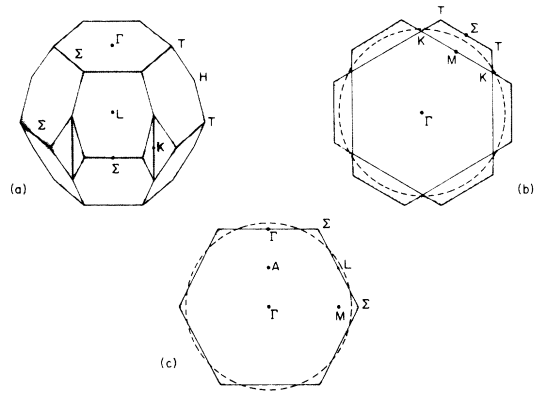

FIG. 4. Fermi surface of beryllium. (a) Occupied volume in reciprocal space: The polyhedron represents the first two Brillouin zones. The dark regions are part of the coronet and cigars. (b) Cut through the basal plane. (c) Cut perpendicular to $\langle 11\bar{2}0 \rangle$ direction. The dashed circles represent the free-electron Fermi sphere.

the second minimum in $\delta(z)$ near $z = 1.0$. We see, therefore, that in beryllium, where the Fermi surface is exceptionally small, the Brillouin-zone structure essentially determines the observed anisotropies. In particular, the large anisotropy at $z = 0$ is a direct consequence of the flattening of the occupied polyhedron along the basal plane, which in turn is related to the bonding anisotropy which is responsible for the anomalous c/a ratio in the crystal structure.

In order to consider the full shape of the valence profile it is necessary to separate the core contribution. Because of the complete overlap of the two, the separation can only be done on theoretical grounds, such as were developed in Sec. IV. In Fig. 2, curve (a) is the arithmetic average of the experimental profiles for the three different directions. Curve (c) is derived directly from Eq. (1) using Clementi's[14] Hartree-Fock Be 1s initial-state wave function and a plane-wave final state. This particular calculation, which exhibits large deviation from the experiment, illustrates the sensitivity of the scattering analysis to the recoil-state specification. The impulse approximation for the core electrons is shown as curve (b). In comparison to the former model it proves to contain a more consistent set of assumptions. The profiles (d) and (e) are the numerical calculations described in Sec. IV, without and with the arbitrary relaxation included, respectively.

In comparing the theoretical core profiles to the data, an important criterion is that subtraction of the theoretical core should leave a roughly symmetrical remainder. Curve (e) is the only one which satisfies that requirement within the previous estimation of experimental error. This result is sur-

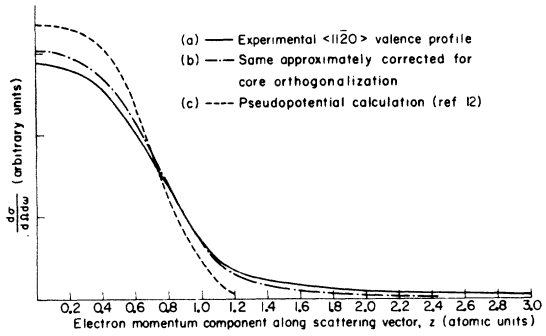

FIG. 5. Experimental $\langle 11\bar{2}0\rangle$ valence profile and pseudopotential calculation.

prising since the assumption of complete relaxation does not seem plausible. One would expect the actual curve to lie somewhere between curves (d) and (e). However, since the amount of asymmetry in the tails of the Compton line is an aspect of the experimental result which might be affected by a systematic bias in the data reduction, we would not wish to overstress that particular comparison.[15]

For consideration of the valence profile, however, the impulse and both numerical results are sufficiently close to one another that it is immaterial which is subtracted, as long as the remainder is symmetrized by averaging the $\pm z$ sides. In any case, the resulting valence distribution exhibits long tails which extend well beyond the free-electron Fermi momentum.

At this time no theoretical calculation accounts for the observed x-ray shape. The free-electron model (not shown) is simply an inverted parabola which falls to zero at $z = 1.03$ a.u. The pseudopotential result[12] is shown as curve (c) in Fig. 5. It contains relatively little in the way of high-momentum components. The positron data are in good agreement with this calculation after the broad slowly varying part of the experimental profile is subtracted.[12] The precise effect of that subtraction on a comparison with the x-ray results is not entirely clear. Nonetheless, assuming both experiments to be correct, we would again expect that deviations might be due to spatial probability density differences, with the resulting implication that valence electrons have higher momenta in the core region. Since the pseudopotential calculation is not expected to simulate adequately the behavior of the valence wave function in the core region, perhaps its better agreement with the positron than with the x-ray result is not surprising.

Part of the effect of the crystal potential can be estimated by imposing the requirement that the valence-electron wave functions be orthogonal to the 1*s* functions. An approximate derivation, based on the use of *one* plane wave for the smooth pseudo-wave-function, yields that the orthogonalization effect is just 8% of the theoretical core profile. Subtraction of that component and renormalization to the full area gives profile (b) in Fig. 5. Within experimental significance, the orthogonalization accounts for the tail beyond ~ 2.2 a.u., but a discrepancy remains in the intermediate region.

A likely source of a tail in the momentum distribution just outside the Fermi surface is electron-electron correlations. While no calculation of this effect in Be metal is available, a calculation for an interacting electron gas of comparable density has been performed in the random-phase approximation.[16] Figure 6 shows the Compton profile derived from this calculation in comparison with the free-electron parabola. By comparing Figs. 5 and 6 we see that the correlation tail as calculated for the electron gas is far smaller than the remaining tail in our Compton profile.

VI. SUMMARY

Qualitative agreement with previous Compton and positron experiments has been found regarding anisotropy in the valence-electron momentum distribution of beryllium. The anisotropy can be explained by simple geometrical considerations, but appears to be smaller in magnitude than is indicated by pseudopotential calculation.

The valence-electron distribution also exhibits significant density at high momenta, well beyond the free-electron Fermi momentum. In view of the

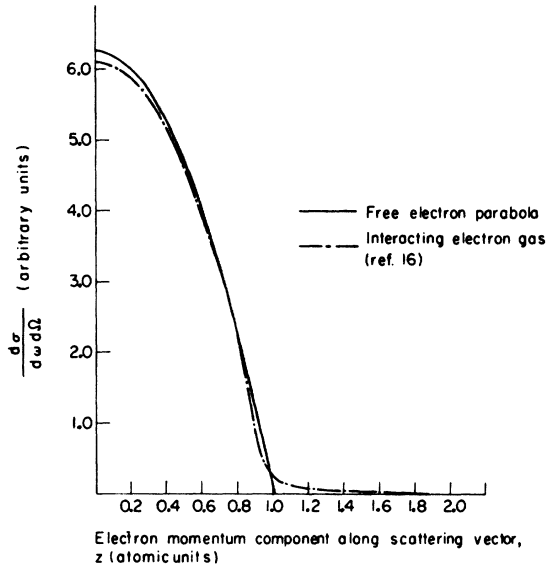

FIG. 6. Comparison between noninteracting (——) and interacting (—— · ——) electron-gas Compton profiles.

electron-gas results it seems unlikely that this effect is produced by electron-electron correlations. Comparison with the positron data suggests that high-momentum components in the electronic wave functions are spatially associated with regions of large core potential. Neither a simple core orthogonalization derivation nor a pseudopotential calculation accounts adequately for the true profile shape. A more detailed calculation appears to be warranted.

The Compton data have been compared with estimates of the core contribution derived on the basis of (a) the "impulse" approximation, using Clementi's[10] 1s wave function, and (b) a free-atom-like numerical calculation, using the Herman-Skillman potential for both the initial and final states. It agrees best, however, with a calculation in which an altered and probably over-relaxed potential is used for the recoil state. Experimental resolution of the details of core electron scattering may require additional data, specifically aimed at measuring the asymmetry in the profile tails.

ACKNOWLEDGMENTS

We wish to acknowledge a number of useful conversations with Walter Phillips and with Richard J. Weiss. We also appreciate the support and interest of B. L. Averbach. This research was sponsored by Advanced Research Projects Agency (Contract No. SD-90), the National Science Foundation (Contract No. GP-7677), and Air Force Materials Laboratory, MAMP (Contract No. F33615-67-C-1226).

*Work based in part on a thesis submitted to the Department of Metallurgy and Materials Science by R. Currat in partial fulfillment of the requirements for the Ph. D. degree.

†Present address: Centre d'Etudes Nucléaires de Grenoble, Cédex 85, 38 Grenoble Gare, France.

[1]W. C. Philipps and R. J. Weiss, Phys. Rev. 171, 790 (1968).

[2]A. T. Stewart, J. B. Shand, J. J. Donaghy, and J. H. Kusmiss, Phys. Rev. 128, 118 (1962).

[3]W. A. Rachinger, J. Sci. Instr. 25, 254 (1948).

[4]I. Waller and D. R. Hartree, Proc. Roy. Soc. (London) A124, 119 (1929).

[5]P. Eisenberger and P. M. Platzman, Phys. Rev. A 2, 415 (1970).

[6]P. D. De Cicco, MIT Solid State and Molecular Theory Group Semiannual Progress Report No. 71, 1969 (unpublished).

[7]W. Heitler, *The Quantum Theory of Radiation*, 3rd ed. (Oxford U. P., London, 1954), p. 217.

[8]H. Gummel and M. Lax, Ann. Phys. (N.Y.) 2, 28 (1957).

[9]F. Herman and S. Skillman, *Atomic Structure Calculations* (Prentice-Hall, Englewood Cliffs, N.J., 1963).

[10]J. H. Terrell, Phys. Rev. 149, 526 (1966).

[11]J. C. Slater, *Quantum Theory of Atomic Structure* (McGraw-Hill, New York, 1960), p. 369.

[12]J. B. Shand, Jr., Phys. Letters 30A, 478 (1969).

[13]T. L. Loucks and P. H. Cutler, Phys. Rev. 133, A819 (1964).

[14]E. Clementi, IBM J. Res. Develop. 9, 2 (1965).

[15]In order to obtain a greater confidence in the measurement of core profile asymmetry, it will probably be necessary to eliminate the background by premonochromating the beam.

[16]D. J. W. Gelbart, A. Houghton, and S. H. Vosko, Can. J. Phys. 42, 1938 (1964).

PHYSICAL REVIEW B VOLUME 3, NUMBER 2 15 JANUARY 1971

Hall Effect in the Pd-H System

R. Wiśniewski and A. J. Rostocki
Institute of Physics, Warsaw Technical University, Warsaw, Poland
(Received 12 June 1970)

The Hall effect of the palladium-hydrogen system has been investigated as a function of the hydrogen content at a temperature of 25 °C. The Hall coefficient rapidly decreases at atomic ratios H/Pd > 0.83. The effective number of electrons per palladium atom for atomic ratio H/Pd > 0.83 was calculated. A high-pressure method of saturation was used.

Recently, with the new capability of obtaining gaseous hydrogen under very high hydrostatic pressures up to 25 kbar [1] and 28 kbar, [2] the relationship between the relative electric resistance R/R_0 and the atomic ratio H/Pd in the Pd-H system for H/Pd > 0.8 has been found. [3] In this investigation the authors took into account the known linear relation between the atomic ratio H/Pd and the logarithm of the hydrogen pressure, valid for the pure β phase, replacing pressure by the hydrogen fugacity. The results of some recent experiments[4] have proved that, in the range of the atomic ratios H/Pd up to 0.97, calculations made on this basis and applied in Ref. 3 were certainly correct. The results ob-

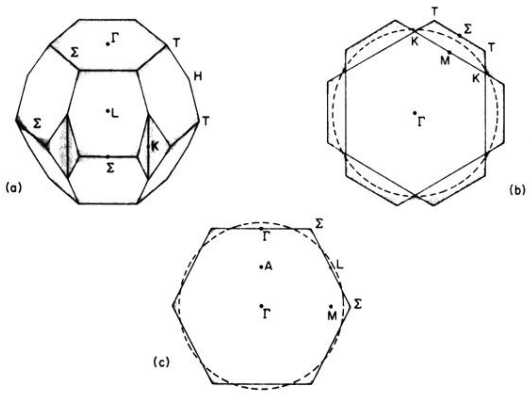

FIG. 4. Fermi surface of beryllium. (a) Occupied volume in reciprocal space: The polyhedron represents the first two Brillouin zones. The dark regions are part of the coronet and cigars. (b) Cut through the basal plane. (c) Cut perpendicular to $\langle 11\bar{2}0 \rangle$ direction. The dashed circles represent the free-electron Fermi sphere.